Eur. Phys. J. E (2015) **38**: 117
DOI 10.1140/epje/i2015-15117-1

THE EUROPEAN PHYSICAL JOURNAL E

Regular Article

Microphase separation patterns in diblock copolymers on curved surfaces using a nonlocal Cahn-Hilliard equation

Darae Jeong and Junseok Kim[a]

Department of Mathematics, Korea University, Seoul 136-713, Republic of Korea

Received 15 May 2015 and Received in final form 8 September 2015
Published online: 20 November 2015 –

Abstract. We investigate microphase separation patterns on curved surfaces in three-dimensional space by numerically solving a nonlocal Cahn-Hilliard equation for diblock copolymers. In our model, a curved surface is implicitly represented as the zero level set of a signed distance function. We employ a discrete narrow band grid that neighbors the curved surface. Using the closest point method, we apply a pseudo-Neumann boundary at the boundary of the computational domain. The boundary treatment allows us to replace the Laplace-Beltrami operator by the standard Laplacian operator. In particular, we can apply standard finite difference schemes in order to approximate the nonlocal Cahn-Hilliard equation in the discrete narrow band domain. We employ a type of unconditionally stable scheme, which was introduced by Eyre, and use the Jacobi iterative to solve the resulting implicit discrete system of equations. In addition, we use the minimum number of grid points for the discrete narrow band domain. Therefore, the algorithm is simple and fast. Numerous computational experiments are provided to study microphase separation patterns for diblock copolymers on curved surfaces in three-dimensional space.

1 Introduction

The directed self-assembly of block copolymers in thin films is an emerging technology for nanoscale patterning (see [1] and references. therein). A diblock copolymer consists of two blocks, each of a different type of monomer, which are joined chemically to each other [2]. When the temperature is lowered below a critical point, the two sequences become incompatible, and the copolymer melt undergoes phase separation. This results in the occurrence of periodic structures such as lamellae, spheres, cylinders, and gyroids [3,4]. Such phase ordering or separation may occur on static or dynamic surfaces [5]. For example, we name the cases of lipid bilayer membranes [6], crystal growth on curved surfaces [7], and phase separation within thin film [8].

The study of "phase separation in confined geometries" has a long history. In this context, many authors [9–12] have considered wetting surfaces, where the kinetic process is referred to as surface-directed spinodal decomposition (SDSD). However, there have also been several studies [4,5,13–16] on neutral surfaces, as will be considered in this work.

Experimental studies in this setting present many challenges, owing to the intrinsic complexity of the block copolymer molecules [14]. Therefore, it is helpful to investigate mathematical models and numerical simulations to understand the dynamics. Although a considerable number of numerical studies [4,13,15,17–20] have focused on microphase separation patterns for diblock copolymers on flat surfaces, there have been few attempts to investigate phase separation on curved surfaces [5,21,22].

In this article, we investigate microphase separation patterns for diblock copolymers on curved surfaces in three-dimensional space using numerical techniques. We adopt a nonlocal Cahn-Hilliard (CH) equation [16] as a mathematical model for block copolymers. The key element in solving the nonlocal CH equation on a surface is calculating the Laplace-Beltrami operator [23], for describing a Laplacian on a curved surface [5]. Our method is based on the closest point method [24], and lets us replace the Laplace-Beltrami operator by the standard Laplacian operator. Given a curved surface, we define a signed distance function to represent the surface as the zero level set of the function [25]. Furthermore, we use the minimum number of a discrete narrow band grid that neighbors the curved surface. Using the finite difference method, we approximate the nonlocal CH equation in the discrete narrow band domain. We employ a type of unconditionally stable scheme, introduced by Eyre [26], and apply the Jacobi iterative method [27] to solve the resulting implicit discrete system of equations. On the computational domain boundary, we apply a pseudo-Neumann boundary condition, by using the closest point method. This boundary treatment results in constant values for the solution along the direction that is normal to the curved

[a] e-mail: cfdkim@korea.ac.kr

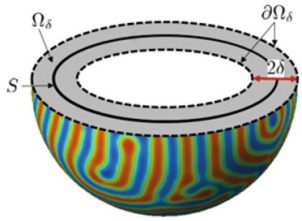

Fig. 1. Schematic illustration of a surface S, a narrow band domain Ω_δ with thickness 2δ, and its boundary $\partial\Omega_\delta$.

surface. Therefore, we can use the standard Laplacian operator instead of the Laplace-Beltrami operator. Thus, the proposed algorithm should be simple and fast. Numerous computational experiments are provided to study microphase separation patterns for diblock copolymers on curved surfaces in three-dimensional space. The numerical results confirm that the proposed algorithm is simple and fast.

The layout of the rest of this paper is as follows. In sect. 2, we describe the nonlocal CH equation on a narrow band domain. In sect. 3, we provide the numerical solution algorithm. We present our numerical results in sect. 4. In sect. 5, some conclusions are delivered.

2 Mathematical model on a narrow band domain

Let S be a given smooth surface embedded in $\mathbb{R}^3$ and $\Omega_\delta = \{\mathbf{y} | \mathbf{x} \in S, \mathbf{y} = \mathbf{x} + \theta\mathbf{n}(\mathbf{x}) \text{ for } |\theta| < \delta\}$ be a δ-neighborhood band of S, where $\mathbf{n}(\mathbf{x})$ is a unit normal vector at $\mathbf{x} \in S$. Figure 1 presents a schematic illustration of S, Ω_δ, and the boundary $\partial\Omega_\delta$ of the narrow band domain Ω_δ.

We consider a diblock copolymer consisting of two homopolymer blocks A and B. Let the order parameter $\phi(\mathbf{x}, t) = \rho_A(\mathbf{x}, t) - \rho_B(\mathbf{x}, t)$ be defined as the difference between the local volume fractions of A and B at position $\mathbf{x}$ and time t. Let $\mathcal{E}_{\text{total}} = \mathcal{E}_{\text{short}} + \mathcal{E}_{\text{long}}$ be the free energy functional of the system, where $\mathcal{E}_{\text{short}}$ is the short-range part of the free energy functional, given by

$$\mathcal{E}_{\text{short}} = \int_\Omega \left(F(\phi(\mathbf{x})) + \frac{\epsilon^2}{2} |\Delta\phi(\mathbf{x})|^2 \right) \mathrm{d}\mathbf{x}$$

and $\mathcal{E}_{\text{long}}$ is the long-range part of the free energy functional, given by

$$\mathcal{E}_{\text{long}} = \frac{\alpha}{2} \int_\Omega \int_\Omega G(\mathbf{x} - \mathbf{y})(\phi(\mathbf{x}) - \bar{\phi})(\phi(\mathbf{y}) - \bar{\phi}) \mathrm{d}\mathbf{y}\, \mathrm{d}\mathbf{x},$$

where G is the Green's function, which has the property $\Delta G(\mathbf{x}-\mathbf{y}) = -\delta(\mathbf{x}-\mathbf{y})$. Here, δ is the Dirac delta function. Then, we have the following continuity equation for the order parameter:

$$\frac{\partial\phi(\mathbf{x}, t)}{\partial t} = -\nabla \cdot \mathcal{J}(\mathbf{x}, t), \tag{1}$$

where $\mathcal{J}(\mathbf{x}, t)$ is a flux, taking the form of the gradient of the functional derivative of the free energy

$$\mathcal{J} = -\nabla\mu. \tag{2}$$

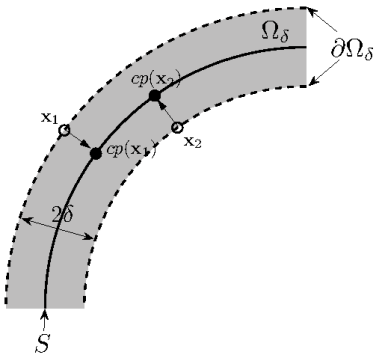

Fig. 2. Closest points $\text{cp}(\mathbf{x}_1)$ and $\text{cp}(\mathbf{x}_2)$ for points $\mathbf{x}_1$ and $\mathbf{x}_2$.

Here, $\mu = \delta\mathcal{E}_{\text{total}}/\delta\phi$. From eqs. (1) and (2), we can obtain the Ohta-Kawasaki model [28]:

$$\frac{\partial\phi(\mathbf{x}, t)}{\partial t} = \Delta\mu(\mathbf{x}, t) - \alpha\left(\phi(\mathbf{x}, t) - \bar{\phi}\right), \tag{3}$$

$$\mu(\mathbf{x}, t) = F'(\phi(\mathbf{x}, t)) - \epsilon^2\Delta\phi(\mathbf{x}, t), \tag{4}$$

where $\mathbf{x} \in \Omega_\delta$, $0 < t \le T$, $F(\phi) = 0.25(\phi^2 - 1)^2$ is a double well potential, ϵ is a positive constant, α is inversely proportional to the square of the total chain length of the copolymer [29], and $\bar{\phi} = \int_{\Omega_\delta} \phi(\mathbf{x}, 0)\mathrm{d}\mathbf{x} / \int_{\Omega_\delta} \mathrm{d}\mathbf{x}$ is the spacial mean value of the order parameter.

The integrands of the short-range and long-range energy functionals are local and nonlocal, respectively. If we only consider the short-range energy functional, then we get the CH equation ($\alpha = 0$ in eq. (3)), which describes the process of the reduction in the total interfacial energy of a microstructure. If $\alpha \neq 0$, then a long-range effect is also present. The minimization of $\mathcal{E}_{\text{short}}$ yields the domains of pure phases with $\phi = \pm 1$, with minimal transition regions; whereas, $\mathcal{E}_{\text{long}}$ induces oscillations between the phases according to the average volume fraction $\bar{\phi}$ [13]. In the context of phase separation with chemical reactions, Puri and Frisch [30] and Glotzer *et al.* [31,32] have noted that the segregation of block copolymers is described by the nonlocal CH equation.

Next, we describe the governing equation on curved surfaces. Let $\text{cp}(\mathbf{x})$ be the point belonging to S that is closest to $\mathbf{x}$ [33]. Figure 2 illustrates the closest points $\text{cp}(\mathbf{x}_1)$ and $\text{cp}(\mathbf{x}_2)$ for boundary points $\mathbf{x}_1$ and $\mathbf{x}_2$, respectively, on $\partial\Omega_\delta$. The boundary condition is given by

$$\phi(\mathbf{x}, t) = \phi(\text{cp}(\mathbf{x}), t) \quad \text{on} \quad \partial\Omega_\delta. \tag{5}$$

Because we want to investigate microphase separation patterns on a curved surface $\mathcal{S}$ in the three-dimensional space $\mathbb{R}^3$, we need to solve the following nonlocal CH equation on the curved surface:

$$\frac{\partial\phi(\mathbf{x}, t)}{\partial t} = \Delta_{\mathcal{S}}\mu(\mathbf{x}, t) - \alpha\left(\phi(\mathbf{x}, t) - \bar{\phi}\right),$$

$$\mu(\mathbf{x}, t) = F'(\phi(\mathbf{x}, t)) - \epsilon^2\Delta_{\mathcal{S}}\phi(\mathbf{x}, t),$$

where $\mathbf{x} \in \mathcal{S}$, and $\Delta_{\mathcal{S}}$ is the Laplace-Beltrami operator.

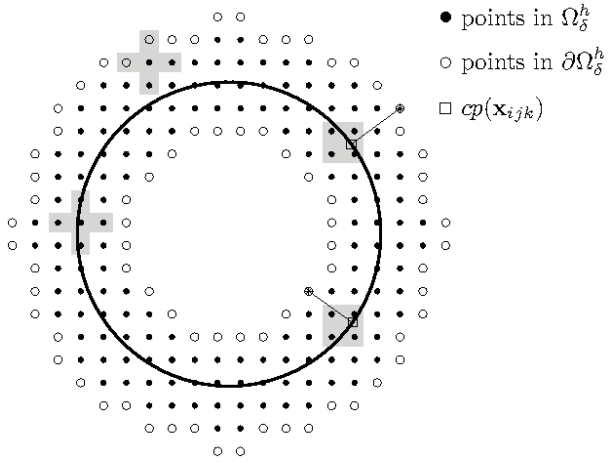

Fig. 3. Schematic illustration of the discrete narrow band domain Ω_δ^h (indicated by •) and its ghost points $\partial\Omega_\delta^h$ (indicated by ○). Here the curve $\mathcal{S}$ is illustrated by the solid line. Cross shaded regions indicate the stencil for the discrete Laplacian. Square shaded regions indicate the interpolation stencil for $\mathrm{cp}(\mathbf{x}_{ijk})$.

For a given smooth surface $\mathcal{S}$, we define a signed distance function $\psi : \mathbb{R}^3 \to \mathbb{R}$ for $\mathcal{S}$. Specifically, $\mathcal{S} = \{\mathbf{x} \in \mathbb{R}^3 : \psi(\mathbf{x}) = 0\}$, with $\psi < 0$ inside of $\mathcal{S}$ and $\psi > 0$ outside of $\mathcal{S}$. The tangential gradient of ϕ on $\mathcal{S}$ can be written as

$$\nabla_{\mathcal{S}}\phi(\mathbf{x},t) = \mathbf{P}(\mathbf{x})\nabla\phi(\mathbf{x},t),$$

where $\mathbf{P} = \mathbf{I} - (\nabla\psi)^T\nabla\psi$ is a projection operator on the tangent space. Here, $\mathbf{I}$ is the 3×3 identity matrix [34]. Then, the Laplace-Beltrami operator is defined as

$$\Delta_{\mathcal{S}}\phi = \nabla_{\mathcal{S}} \cdot \nabla_{\mathcal{S}}\phi = (\mathbf{P}\nabla) \cdot (\mathbf{P}\nabla\phi) = \nabla \cdot (\mathbf{P}\nabla\phi).$$

If we take a small enough δ, then the numerical solution of eqs. (3) and (4), with the boundary condition (5) yields a ϕ that is constant along the direction that is normal to the surface. Thus, we can use the standard Laplacian operator instead of the Laplace-Beltrami operator in the narrow band domain.

3 Numerical solution algorithm

In this section, we describe our algorithm for a numerical solution to the nonlocal CH equation on the narrow band domain, Ω_δ. We discretize the nonlocal CH equation in a three-dimensional domain $\Omega = (a,b) \times (c,d) \times (e,f)$ that includes Ω_δ. Let $h = (b-a)/N_x = (d-c)/N_y = (f-e)/N_z$ be the uniform mesh size, where N_x, N_y, and N_z are positive integers. Then $\Omega^h = \{\mathbf{x}_{ijk} = (x_i, y_j, z_k) : x_i = a + hi,\ y_j = c + hj,$ and $z_k = e + hk$ for $0 \le i \le N_x,\ 0 \le j \le N_y,$ and $0 \le k \le N_z\}$ is the discrete domain. Let ϕ_{ijk}^n and μ_{ijk}^n be approximations of $\phi(x_i, y_j, z_k, n\Delta t)$ and $\mu(x_i, y_j, z_k, n\Delta t)$, respectively, where $\Delta t = T/N_t$ is the time step, T is the final time, and N_t is the total number of time steps. We define $\Omega_\delta^h = \{\mathbf{x}_{ijk} : |\psi_{ijk}| < \delta\}$ as the discrete narrow band domain (see fig. 3). We need to take $\delta > \sqrt{3}h$ (the diagonal of a cube with an edge length of h) because Ω_δ^h must contain the interpolation stencil for the closest points of all domain boundary points.

Let $\partial\Omega_\delta^h = \{(x_i, y_j, z_k) : I_{ijk}|\nabla_h I_{ijk}| \neq 0\}$ be the discrete domain boundary points (see fig. 3), where $\nabla_h I_{ijk} = (I_{i+1,jk} - I_{i-1,jk}, I_{i,j+1,k} - I_{i,j-1,k}, I_{ij,k+1} - I_{ij,k-1})/(2h)$. Here, $I_{ijk} = 0$ if $(x_i, y_j, z_k) \in \Omega_\delta^h$, and $I_{ijk} = 1$ otherwise. We consider the following unconditionally stable discretization of the nonlocal CH system given in (3) and (4):

$$\frac{\phi_{ijk}^{n+1} - \phi_{ijk}^n}{\Delta t} = \Delta_h\mu_{ijk}^{n+1} - \alpha\left(\phi_{ijk}^{n+1} - \bar{\phi}\right), \tag{6}$$

$$\mu_{ijk}^{n+1} = \left(\phi_{ijk}^{n+1}\right)^3 - \phi_{ijk}^n - \epsilon^2\Delta_h\phi_{ijk}^{n+1}, \tag{7}$$

where the seven-point discrete Laplacian operator is defined as

$$\Delta_h\phi_{ijk} = \frac{\phi_{i+1,jk} + \phi_{i-1,jk} + \phi_{i,j+1,k} + \phi_{i,j-1,k}}{h^2} + \frac{\phi_{ij,k+1} + \phi_{ij,k-1} - 6\phi_{ijk}}{h^2}.$$

The pseudo-Neumann boundary condition on $\partial\Omega_\delta^h$ is implemented as

$$\phi_{ijk}^{n+1} = \phi^{n+1}(\mathrm{cp}(\mathbf{x}_{ijk})) \quad \text{and} \quad \mu_{ijk}^{n+1} = \mu^{n+1}(\mathrm{cp}(\mathbf{x}_{ijk})).$$

Let $\mathbf{x}_{ijk}$ be a boundary point in $\partial\Omega_\delta^h$. Then,

$$\mathrm{cp}(\mathbf{x}_{ijk}) = \mathbf{x}_{ijk} - \frac{\nabla_h|\psi_{ijk}|}{|\nabla_h|\psi_{ijk}||}|\psi_{ijk}|$$

is the numerical closest point to the surface $\mathcal{S}$. In general, $\mathrm{cp}(\mathbf{x}_{ijk})$ is not a grid point in the discrete narrow band domain, *i.e.*, $\mathrm{cp}(\mathbf{x}_{ijk}) \notin \partial\Omega_\delta^h$. Therefore, we calculate $\phi^n(\mathrm{cp}(\mathbf{x}_{ijk}))$ by using trilinear interpolation (see fig. 3). Using the Jacobi iteration method, we solve eqs. (6) and (7) numerically. Assume that we have the numerical solution at time step level n, ϕ_{ijk}^n. Then, we want to find the numerical solution ϕ_{ijk}^{n+1} at time level $n+1$. First, we take an initial guess $\phi_{ijk}^{n+1,1} = \phi_{ijk}^n$ and $\mu_{ijk}^{n+1,1} = \mu_{ijk}^n$. Then, we apply the Jacobi iteration defined by (8) and (9) for eqs. (6) and (7), until the stopping criterion is satisfied, $\|\phi^{n+1,m+1} - \phi^{n+1,m}\|_{L^2(\Omega_\delta^h)} < \mathrm{tol}$, where "tol" is a given tolerance value. Here, a discrete L^2-norm on Ω_δ^h is defined as $\|\phi\|_{L^2(\Omega_\delta^h)} = \sqrt{\sum_{\mathbf{x}_{ijk}\in\Omega_\delta^h}\phi_{ijk}^2/\#\Omega_\delta^h}$, where $\#\Omega_\delta^h$ is the number of elements of the set Ω_δ^h. By $\phi^{n+1,m}$ and $\phi^{n+1,m+1}$, we denote the iterative solutions after the m-th and $(m+1)$-th rounds of Jacobi iteration. The Jacobi

iteration is given by

$$\left(\frac{1}{\Delta t}+\alpha\right)\phi_{ijk}^{n+1,m+1}+\frac{6}{h^2}\mu_{ijk}^{n+1,m+1}= \frac{\phi_{ijk}^{n}}{\Delta t}+\alpha\bar{\phi}+\frac{1}{h^2}\left(\mu_{i+1,jk}^{n+1,m}+\mu_{i-1,jk}^{n+1,m}+\mu_{i,j+1,k}^{n+1,m}\right) +\frac{1}{h^2}\left(\mu_{i,j-1,k}^{n+1,m}+\mu_{ij,k+1}^{n+1,m}+\mu_{ij,k-1}^{n+1,m}\right), \quad (8)$$

$$-\left(3\left(\phi_{ijk}^{n+1,m}\right)^2+\frac{6\epsilon^2}{h^2}\right)\phi_{ijk}^{n+1,m+1}+\mu_{ijk}^{n+1,m+1}= -\phi_{ijk}^{n}+2\left(\phi_{ijk}^{n+1,m}\right)^3+\frac{\epsilon^2}{h^2}\left(\phi_{i+1,jk}^{n+1,m}+\phi_{i-1,jk}^{n+1,m}\right) +\frac{\epsilon^2}{h^2}\left(\phi_{i,j+1,k}^{n+1,m}+\phi_{i,j-1,k}^{n+1,m}+\phi_{ij,k+1}^{n+1,m}+\phi_{ij,k-1}^{n+1,m}\right), \quad (9)$$

for all $\mathbf{x}_{ijk}\in\Omega_\delta^h$. Equations (8) and (9) can be rewritten in the following form:

$$\begin{pmatrix} a & b\\ c & 1\end{pmatrix}\begin{pmatrix}\phi_{ijk}^{n+1,m+1}\\ \mu_{ijk}^{n+1,m+1}\end{pmatrix}=\begin{pmatrix} f\\ g\end{pmatrix},$$

where

$$a=\frac{1}{\Delta t}+\alpha,\qquad b=\frac{6}{h^2},\qquad c=-3\left(\phi_{ijk}^{n+1,m}\right)^2-\frac{6\epsilon^2}{h^2},$$

$$f=\frac{\phi_{ijk}^{n}}{\Delta t}+\alpha\bar{\phi}+\frac{1}{h^2}\left(\mu_{i+1,jk}^{n+1,m}+\mu_{i-1,jk}^{n+1,m}+\mu_{i,j+1,k}^{n+1,m}\right) +\frac{1}{h^2}\left(\mu_{i,j-1,k}^{n+1,m}+\mu_{ij,k+1}^{n+1,m}+\mu_{ij,k-1}^{n+1,m}\right),$$

$$g=-\phi_{ijk}^{n}+2\left(\phi_{ijk}^{n+1,m}\right)^3+\frac{\epsilon^2}{h^2}\left(\phi_{i+1,jk}^{n+1,m}+\phi_{i-1,jk}^{n+1,m}\right) +\frac{\epsilon^2}{h^2}\left(\phi_{i,j+1,k}^{n+1,m}+\phi_{i,j-1,k}^{n+1,m}+\phi_{ij,k+1}^{n+1,m}+\phi_{ij,k-1}^{n+1,m}\right).$$

Therefore, the solutions at each step are obtained as

$$\phi_{ijk}^{n+1,m+1}=\frac{f-bg}{a-bc}\quad\text{and}\quad\mu_{ijk}^{n+1,m+1}=\frac{ag-cf}{a-bc}.$$

In each updating step, we define the boundary points using the closest point method and trilinear interpolation. Note that we only use the closest point method on the boundary points, not on the narrow band domain.

4 Numerical experiments

In this section, we perform several numerical experiments on various curved surfaces.

4.1 Comparison with previous numerical results

In order to verify our proposed numerical scheme, we perform the same numerical tests as in [5], where Tang *et al.* studied phase separation on spherical surfaces by solving the nonlocal CH equation using a finite volume method. They found that at a late stage of phase separation for a symmetric composition of the block copolymers, spiral structures are seen on the spherical surface, which has not been observed to occur on a flat surface. To be consistent with the previous tests, we set $\epsilon=1$, $h=1$, and $\Delta t=1$ on the computational domain $\Omega=[-37.5,37.5]^3$. The sphere surface is represented by the zero level set of the signed distance function

$$d(x,y,z)=\sqrt{x^2+y^2+z^2}-31.25. \quad (10)$$

For the first test, we perform a numerical simulation with $\alpha=0.2$ and an initial condition of $\phi(x,y,z)=0.5\,\mathrm{rand}(x,y,z)$, where $\mathrm{rand}(x,y,z)$ is a uniformly distributed random number between -1 and 1. For comparison, we include reprinted images from [5] in fig. 4(a). Figure 4(b) shows the temporal evolution of morphological patterns during spinodal decomposition on the sphere. In this figure, we can see that our results show a similar lamella pattern to that in fig. 4(a).

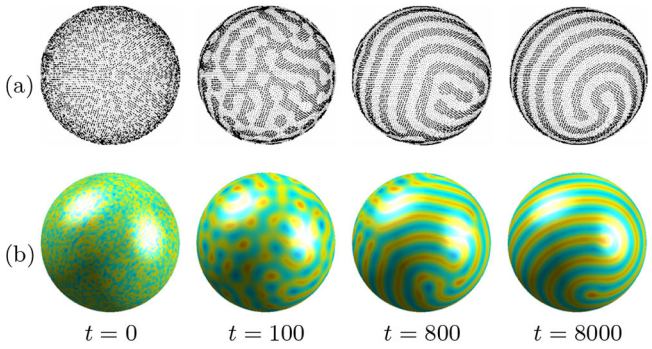

Fig. 4. Temporal evolutions of lamella pattern on the sphere surface with initial conditions $\phi(x,y,z)=0.5\,\mathrm{rand}(x,y,z)$ and $\alpha=0.2$. Here, $\mathrm{rand}(x,y,z)$ is random value between -1 and 1. (a) Reprinted images from Tang *et al.* [5]. © 2005, American Physical Society. Reprinted with permission. (b) Numerical results obtained using our proposed method. The computational times are shown below each column.

Figure 5 shows the temporal evolution of morphological patterns during spinodal decomposition on the surface of the sphere with $\alpha=0.1$ and the initial condition $\phi(x,y,z)=-0.3+0.5\,\mathrm{rand}(x,y,z)$. From a random initial state, the phase on the sphere separates into a hex-cylinder type phase, as shown in fig. 5(b), which is similar to the previous result from fig. 5(a) in Tang *et al.* [5].

4.2 Temporal evolution on a torus

Our next example is that of phase separation on the surface of a torus. The torus is represented by the zero level set of the signed distance function as follows:

$$d(x,y,z)=\sqrt{(\sqrt{x^2+y^2}-0.7)^2+z^2}-0.3. \quad (11)$$

Figures 6(a) and (b) show the phase separation on the surface of a torus with two initial conditions: (a)

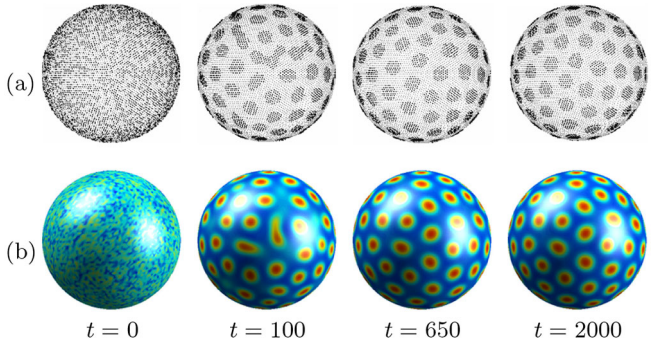

Fig. 5. Temporal evolutions of hexagonal patterns on the sphere surface with initial conditions $\phi(x, y, z) = -0.3 + 0.5\,\mathrm{rand}(x, y, z)$ and $\alpha = 0.1$. (a) Reprinted images from Tang *et al.* [5]. © 2005, American Physical Society. Reprinted with permission. (b) Numerical results obtained using our proposed method. The computational times are shown below each column.

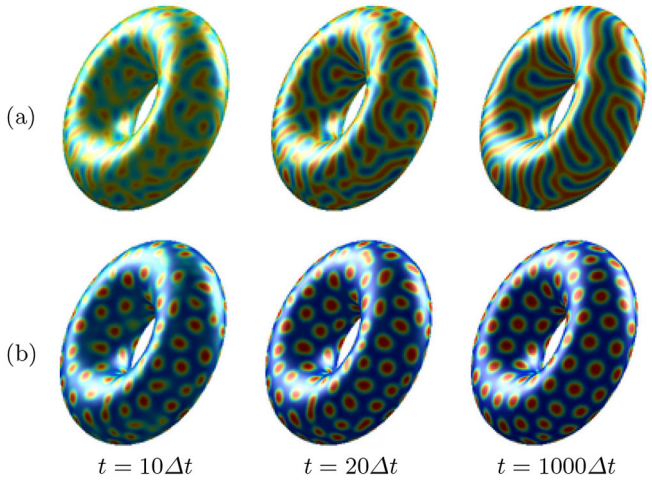

Fig. 6. Phase separation on torus. Temporal evolutions with (a) $\phi(x, y, z, 0) = 0.0 + 0.5\,\mathrm{rand}(x, y, z)$, $\epsilon = 1/(20\sqrt{2})$, $h = 0.0375$ and (b) $\phi(x, y, z, 0) = -0.3 + 0.5\,\mathrm{rand}(x, y, z)$, $\epsilon = 1/(30\sqrt{2})$, and $h = 0.031$. The computational times are shown below each column.

$\phi(x, y, z, 0) = 0.0 + 0.5\,\mathrm{rand}(x, y, z)$, $\epsilon = 1/(20\sqrt{2})$, $h = 0.0375$, $N_x = N_y = N_z = 51$, $\Delta t = 0.1$ and (b) $\phi(x, y, z, 0) = -0.3 + 0.5\,\mathrm{rand}(x, y, z)$, $\epsilon = 1/(30\sqrt{2})$, $\Delta t = 0.1$, $h = 0.031$, $N_x = N_y = N_z = 51$, $\Delta t = 0.1$, respectively. Depending on the values of the parameters, the phase on the torus forms different patterns. As shown in figs. 6(a) and (b), we have lamellar and hexagonal patterns, respectively. The required computational times are shown below each column.

4.3 Temporal evolution on a cube

Now, we demonstrate the robustness of the proposed numerical algorithm by performing phase separation simulation on a cube surface, which has sharp curvatures. Here,

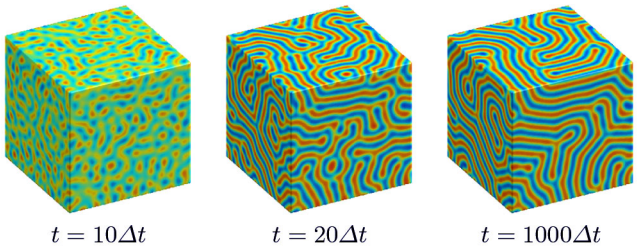

Fig. 7. Phase separation on a cube surface. Temporal evolutions with $\phi(x, y, z, 0) = 0.0 + 0.5\,\mathrm{rand}(x, y, z)$, $\epsilon = 1/(20\sqrt{2})$, and $h = 0.0375$. The computational times are shown below each figure.

the cube surface is represented by the zero level set of the signed distance function as follows:

$$d(x, y, z) = \min\left(\max\left(\bar{x}, \max(\bar{y}, \bar{z})\right), 0\right) + \sqrt{\max(\bar{x}, 0)^2 + \max(\bar{y}, 0)^2 + \max(\bar{z}, 0)^2}, \tag{12}$$

where $\bar{x} = |x| - 1.7$, $\bar{y} = |y| - 1.7$, and $\bar{z} = |z| - 1.7$.

Figure 7 illustrates the temporal evolutions of phase separation on a cube surface. In this test, we applied an initial condition of $\phi(x, y, z, 0) = 0.0 + 0.5\,\mathrm{rand}(x, y, z)$. The numerical parameters were set to $\epsilon = 1/(20\sqrt{2})$, $\alpha = 100$, $h = 0.0375$, $\Delta t = 0.1$, and $\Omega = [0, 100h]^3$. In fig. 7, the numerical solutions show the development of a lamellar pattern on the cube surface as time progressed. The phase field method that we are currently using is known as treating a microscopically sharp interface like a diffuse region. That is, the phase field variable ϕ is smoothly set to any value from $\phi \approx -1$ to $\phi \approx 1$ between the two phases over the diffuse interface region, which has a small but numerically resolvable thickness. Therefore, we can see stable numerical solutions at sharp curvatures without any difficulties.

4.4 Temporal evolution on a bunny

To demonstrate that our proposed method can deal with complex surfaces, we perform phase separation on the surface of a bunny. For the majority of complex surfaces, closed-form signed distance functions such as eqs. (10), (11), and (12) are not available. Therefore, we need to reconstruct a signed distance function from scattered data points that are sampled from a three-dimensional object. In [35, 36], the authors proposed numerical algorithms for implicit surface reconstruction based on partial differential equations. The method consists of three steps. First, we determine the distance function to a scattered data point set on rectangular grids. Second, we find a good initial surface. Third, we solve time-dependent partial differential equations for the signed distance function. For more details on the numerical algorithm, see [35, 36] and references therein. Figures 8(a)

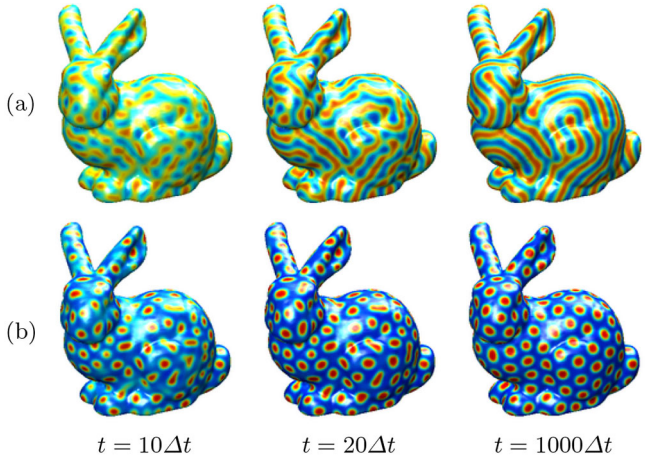

Fig. 8. Morphological evolutions on the surface of a bunny with initial conditions (a) $\phi(x, y, z) = 0.0 + 0.5\,\mathrm{rand}(x, y, z)$ and (b) $\phi(x, y, z) = -0.3 + 0.5\,\mathrm{rand}(x, y, z)$. The computational times are shown below each column.

and (b) demonstrate the temporal evolution of morphological patterns during spinodal decomposition on the surface of the bunny with the initial conditions: $\phi(x, y, z) = 0.0 + 0.5\,\mathrm{rand}(x, y, z)$ and $\phi(x, y, z) = -0.3 + 0.5\,\mathrm{rand}(x, y, z)$, respectively. Here, we set $\Delta t = 0.1$, $\alpha = 100$, and $\Omega = [0, 137h]^3$. For test (a), we used the parameters $h = 0.0375$ and $\epsilon = 1/(20\sqrt{2})$ and for (b), we used $h = 0.031$ and $\epsilon = 1/(30\sqrt{2})$. These specific values are from the same as those used in [15]. From these results we can confirm that the proposed algorithm can compute microphase separation patterns in diblock copolymers on complex surfaces.

4.5 Effect of surface geometry on pattern formation

Finally, we investigate the effect of surface geometry on pattern formation. We consider a torus with the following signed distance function:

$$d(x, y, z) = \sqrt{(\sqrt{x^2 + y^2} - 1)^2 + z^2} - r, \qquad (13)$$

where r is the tube radius of the torus. Here, the torus generated in eq. (13) has a unit circumferential radius, which is the radius of the circle that constitutes the center of the torus tube. We investigate the pattern in a steady state on three different torus surfaces with $r = 0.16$, $r = 0.08$, and 0.03. For our numerical test, we use $h = 0.01$, $\Delta t = 0.001$, $\epsilon = 0.0236$, and $\alpha = 100$ on $\Omega = [-0.5, 0.5]^3$. Figure 9 shows the phase pattern in a steady state on the different tori, with the initial condition $\phi(x, y, z) = \bar{\phi} + 0.5\,\mathrm{rand}(x, y, z)$. For (a) and (b) we applied $\bar{\phi} = 0.0$ and -0.3, respectively. In these numerical results, we obseve lamella and hexagonal patters on the surfaces of the various tori with respect to average concentration. However, when the radius of the torus tube is small, the pattern shows a lamella phase.

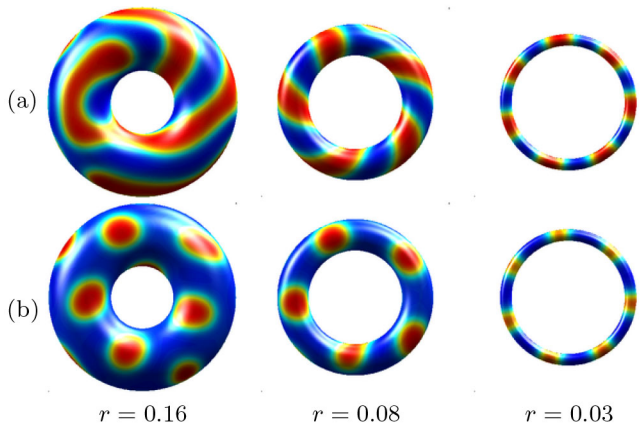

Fig. 9. Phase pattern in a steady state on surface of a torus defined by the signed distance function $d(x, y, z) = \sqrt{(\sqrt{x^2 + y^2} - 1)^2 + z^2} - r$. In this test, the different average concentrations are applied (a) $\bar{\phi} = 0$ and (b) $\bar{\phi} = -0.3$ with the initial condition $\phi(x, y, z) = \bar{\phi} + 0.5\,\mathrm{rand}(x, y, z)$. The other parameters used are $h = 0.01$, $\Delta t = 0.001$, $\epsilon = 0.0236$, and $\alpha = 100$. In addition, each column applied a different radius to the torus tube with $r = 0.16$, $r = 0.08$, and $r = 0.03$, respectively.

5 Conclusions

In this paper, we explored the microphase separation of diblock copolymers on curved surfaces in three-dimensional space. Our study was based on a nonlocal Cahn-Hilliard equation, which is derived from the Ohta-Kawasaki functional. In performing numerical simulations, we implicitly represented curved surfaces as the zero level sets of signed distance functions. By using the standard finite difference scheme, we approximated the nonlocal CH equation in the discrete narrow band domain, which is a neighboring region of the curved surface. In addition, we applied a pseudo-Neumann boundary condition at the boundary of the computational domain using the closet point method. With this treatment of the boundary condition, we were able to replace the Laplace-Beltrami operator with the well-known standard Laplacian operator. The resulting implicit discrete system, obtained from a type of unconditionally stable scheme proposed by Eyre, was solved using the Jacobi iterative method. Because the computation is only performed in a discrete narrow band, the numerical simulation is fast, and its corresponding algorithm is simple. Using this efficient numerical method, we provided several computational experiments to study the patterns of microphase separation for diblock copolymers on various curved surfaces. Through our numerical tests, we found two different patterns on general surfaces: lamella phases for compositionally symmetric block copolymers and hexagonal phases for asymmetric compositions. In particular, we were able to observe the spiral lamella phase, the occurrence of which is not observed in two-dimensional flat space. In addition, in case of torus surfaces with a small tube

radius, we observed a lamellar phase, even though the average concentration $\bar{\phi}$ was not symmetric.

Author contribution statement

All authors contributed extensively to the work presented in this paper. J.S. Kim conceived this study and provided new numerical techniques; D. Jeong performed and analyzed the simulation studies; J.S. Kim and D. Jeong wrote the manuscript and made manuscript revisions.

Author D. Jeong was supported by Basic Science Research Program through the National Research Foundation of Korea (NRF) funded by the Ministry of Education, Science and Technology (2014R1A6A3A01009812). The corresponding author, J.S. Kim, was supported by the National Research Foundation of Korea (NRF) grant funded by the Korea government (MSIP) (NRF-2014R1A2A2A01003683). The authors are grateful to the reviewers whose valuable suggestions and comments significantly improved the quality of this paper.

References

1. I.P. Campbell, G.J. Lau, J.L. Feaver, M.P. Stoykovich, Macromolecules **45**, 1587 (2012).
2. C. Singh, M. Goulian, A.J. Liu, G.H. Fredrickson, Macromolecules **27**, 2974 (1994).
3. F. Liu, N. Goldenfeld, Phys. Rev. A **39**, 4805 (1989).
4. R. Choksi, M.A. Peletier, J.F. Williams, SIAM J. Appl. Math. **69**, 1712 (2009).
5. P. Tang, F. Qiu, H. Zhang, Y. Yang, Phys. Rev. E **72**, 016710 (2005).
6. T. Baumgart, S.T. Hess, W.W. Webb, Nature **425**, 821 (2003).
7. A.R. Bausch, M.J. Bowick, A. Cacciuto, A.D. Dinsmore, M.F. Hsu, D.R. Nelson, M.G. Nikolaides, A. Travesset, D.A. Weitz, Science **299**, 1716 (2003).
8. P. Sens, S.A. Safran, Eur. Phys. J. E **1**, 237 (2000).
9. K. Binder, S. Puri, S.K. Das, J. Horbach, J. Stat. Phys. **138**, 51 (2010).
10. G. Brown, A. Chakrabarti, J. Chem. Phys. **102**, 1440 (1995).
11. K. Binder, J. Non-Equil. Thermodyn. **23**, 1 (1998).
12. H. Xiang, K. Shin, T. Kim, S.I. Moon, T.J. McCarthy, T.P. Russell, Macromolecules **37**, 5660 (2004).
13. R. Choksi, M. Maras, J.F. Williams, SIAM J. Appl. Dyn. Syst. **10**, 1344 (2011).
14. M. Pinna, A.V. Zvelindovsky, Eur. Phys. J. B **85**, 1 (2012).
15. D. Jeong, J. Shin, Y. Li, Y. Choi, J.-H. Jung, S. Lee, J. Kim, Curr. Appl. Phys. **14**, 1263 (2014).
16. R. Choksi, X. Ren, J. Stat. Phys. **113**, 151 (2003).
17. S.W. Sides, G.H. Fredrickson, Polymer **44**, 5859 (2003).
18. S.W. Sides, B.J. Kim, E.J. Kramer, G.H. Fredrickson, Phys. Rev. Lett. **96**, 250601 (2006).
19. K.Ø. Rasmussen, G. Kalosakas, J. Polym. Sci. Pol. Phys. **40**, 1777 (2002).
20. H.D. Ceniceros, G.H. Fredrickson, Multiscale Model. Simul. **2**, 452 (2004).
21. B. Shahriari, PhD thesis, Simon Fraser Univeristy (2010).
22. T.L. Chantawansri, A.W. Bosse, A. Hexemer, H.D. Ceniceros, C.J. García-Cervera, E.J. Kramer, G.H. Fredrickson, Phys. Rev. E **75**, 031802 (2007).
23. I. Chavel, *Eigenvalues in Riemannian Geometry*, Vol. **115** (Academic Press, London, 1984).
24. C.B. Macdonald, S.J. Ruuth, J. Sci. Comput. **35**, 219 (2008).
25. S. Osher, R.P. Fedkiw, J. Comput. Phys. **169**, 463 (2001).
26. D.J. Eyre, in *MRS Proceedings*, Vol. **529** (Cambridge University Press, 1998) p. 39.
27. I.N. Bronshtein, K.A. Semendyayev, *Handbook of Mathematics*, 3rd edition (Springer-Verlag, New York, 1997) p. 892.
28. T. Ohta, K. Kawasaki, Macromolecules **19**, 2621 (1986).
29. Y. Nishiura, I. Ohnishi, Phys. D **84**, 31 (1995).
30. S. Puri, H.L. Frisch, J. Phys. A **27**, 6027 (1994).
31. S. Glotzer, D. Stauffer, N. Jan, Phys. Rev. Lett. **72**, 4109 (1994).
32. S. Glotzer, E.A. Di Marzio, M. Muthukumar, Phys. Rev. Lett. **74**, 2034 (1995).
33. C.B. Macdonald, J. Brandman, S.J. Ruuth, J. Comput. Phys. **230**, 7944 (2011).
34. J.B. Greer, J. Sci. Comput. **29**, 321 (2006).
35. H.-K. Zhao, S. Osher, R. Fedkiw, in *Proceedings of the IEEE Workshop on Variational and Level Set Methods*, Washington, DC, 2001, edited by A.D. Williams (IEEE Comput. Soc., Los Alamitos, 2001) p. 194.
36. H.-K. Zhao, S. Osher, B. Merriman, M. Kang, Comput. Vis. Image Und. **80**, 295 (2000).